Global Energy Interconnection xxx (2026) xxx–xxx

KeAi CHINESE ROOTS GLOBAL IMPACT

Global Energy Interconnection Development and Cooperation Organization

Global Energy Interconnection

Contents lists available at ScienceDirect

journal homepage: www.elsevier.com/locate/gloei

Research on parameter identification of photovoltaic model based on improved crested porcupine optimizer

Hao Guo, Chongru Liu *

State Key Laboratory of Alternate Electrical Power System with Renewable Energy Source (North China Electric Power University), Changping District, Beijing 102206, P.R. China

Received 23 May 2025; revised 1 September 2025; accepted 15 September 2025

Abstract

Precision modeling of photovoltaic systems is essential for technological progress in solar energy applications. To achieve precise extraction of model parameters and enhance photovoltaic model precision, an Improved Crested Porcupine Optimizer (ICPO) incorporating chaotic initialization and Lévy flight perturbations is proposed and applied to PV model parameter extraction. This algorithm solves optimization problems by simulating porcupines' defense behaviors. It introduces chaotic mapping initialization to avoid initial solution differences affecting optimization and identifies underperforming agents with Levy flight perturbations to evade local optima, significantly accelerating convergence and enhancing global optimization ability. Finally, comparative experiments were conducted with various existing methods under different models and data, fully verifying the superiority of the proposed method.

Keywords: Photovoltaic model; Parameter identification; Chaotic mapping; Levy flight; Crested porcupine optimizer algorithm

0 Introduction

The past decade has witnessed accelerated expansion in clean energy, driven by diminishing fossil fuel reserves and increasingly critical environmental challenges like global warming. With photovoltaic installations exhibiting persistent global growth [1], research increasingly focuses on maximizing solar energy utilization efficiency and quantifying system-level integration impacts [2]. It is necessary to construct high-precision photovoltaic models. Within equivalent circuit representations, the predominant approaches are the single and double diode models; precise identification of their parameters is critical for optimizing model fidelity [3].

Global research on PV model parameter identification has formed a solid foundation, with methodologies mainly divided into deterministic and heuristic methods. Deterministic methods include analytical and iterative approaches. The analytical method utilizes PV data table information or its I-V characteristic curves to perform dimensionality reduction search [4], based on Lambert-W [5], and OSMP [6] methods for parameter extraction. Although this method is simple and fast, it often has significant discrepancies between its simulation performance and actual performance; parameter extraction via the iterative method employs established numerical techniques, including the Newton-Raphson approach [7], the Gauss-Seidel algorithm [8], and the least squares method [9,10]. This approach mandates that the system exhibit convexity, continuity, and differentiability, alongside high sensitivity to initial value selection. Literature indicates its accuracy in photovoltaic model parameter identification is typically modest.

Given the shortcomings of deterministic methods, researchers have shifted focus to heuristic approaches

Peer review under the responsibility of Global Energy Interconnection Group Co. Ltd.

* Corresponding author.
E-mail address: chongru.liu@ncepu.edu.cn (C. Liu).

https://doi.org/10.1016/j.gloei.2025.09.008

Please cite this article in press as: H. Guo and C. LiuResearch on parameter identification of photovoltaic model based on improved crested porcupine optimizer. *Global Energy Interconnection* (2026), https://doi.org/10.1016/j.gloei.2025.09.008

[11–14], which use optimization algorithms for parameter identification [15–18]. These methods are widely applied in photovoltaic model parameter identification, including the Reinforcement Learning Knowledge Acquisition Sharing Algorithm (RLGSK) [19], the Three-Point Combined Differential Evolution Algorithm (DE3P) [20], the Teaching–Learning–based Artificial Bee Colony (TLABC) [21], the Generalized Oppositional Teaching Learning Based Optimization (GOTLBO) [22], the Hybrid Nelder-Mead and Modified Particle Swarm Optimization (NM-MPSO) [23], the Directional Permutation Differential Evolution (DPDE) [24], the Whippy Harris Hawks Optimization (WHHO) [25], the mproved JAYA algorithm based on chaos theory (CIJAYA) [26], the improved and simplified teaching–learning based optimization algorithm (STLBO) [27], and the improved tunicate swarm optimization (ITSO) [28].

Introduced in 2024, the Crested Porcupine Optimizer (CPO) demonstrates exceptional efficacy as a novel *meta*-heuristic approach. This algorithm solves optimization problems by simulating various defensive behaviors of the crested porcupine, achieving significantly better results than other algorithms on multiple test functions and engineering problems [29]. However, photovoltaic models exhibit implicit function characteristics and pronounced nonlinearity, frequently causing extended convergence durations and a propensity to become trapped in local optima during optimization. Therefore, this paper incorporates chaotic mapping initialization and Levy flight perturbation to elevate the algorithm's convergence rate and bolster its global optimization efficacy. We establish an Improved Crested Porcupine Optimizer (ICPO) and benchmark its performance across four distinct parameter identification scenarios: encompassing both single-diode and double-diode model types applied to solar cell and photovoltaic module configurations. These results were compared with various novel optimization algorithms widely used in applications and other improved methods from existing literature, thereby validating the superiority and effectiveness of the proposed methodology.

1 Photovoltaic model

Photovoltaic devices are made of semiconductor materials, and their I-V characteristics are similar to the exponential characteristics of diode I-V curve. Therefore, the mathematical model based on diode has been widely recognized and applied. As schematized in Fig. 1, the circuit architecture comprises a current source, a diode, and two resistors arranged in series and parallel configurations.

1.1 Single diode solar cell model

The single diode model (SDM) features notable structural simplicity and enjoys broad adoption. As depicted in Fig. 1(a), the model's topology produces the following output current:

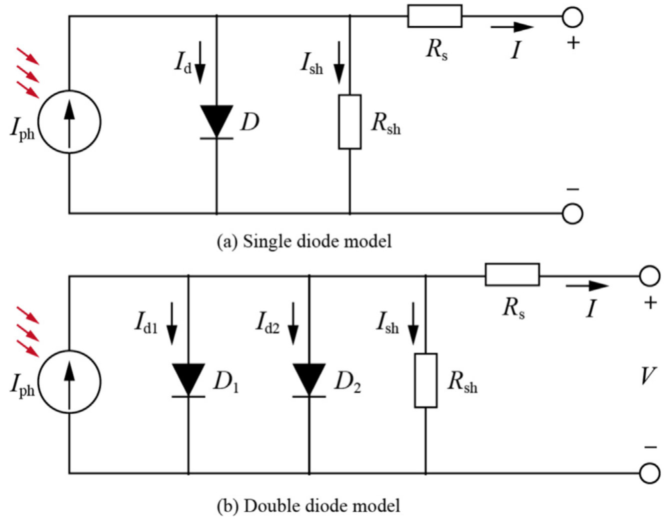

Fig. 1. Equivalent circuit diagram of photovoltaic model.

$$I = I_{ph} - I_{sd}\left[\exp\left(\frac{q(V + IR_s)}{nkT}\right) - 1\right] - \frac{V + IR_s}{R_{sh}} \tag{1}$$

where: I_{ph} denotes the photocurrent generated via the photoelectric effect, while I_{sd} represents the diode saturation current under reverse bias conditions; R_s and R_{sh} denote series and parallel resistance values; V signifies the output terminal voltage; n indicates the diode ideality factor; q denotes the elementary electron charge; k represents the Boltzmann constant; T corresponds to the battery's absolute temperature.

The single diode model requires identification of five parameters: I_{ph}, I_{sd}, R_s, R_{sh} and n.

1.2 Model of double diode solar cell

The double diode model (DDM) accounts for recombination current losses within the depletion region, enabling more precise characterization of solar cell output characteristics. As depicted in Fig. 1(b), the model's topology produces the following output current:

$$\begin{aligned} I = I_{ph} - I_{sd1}\left[\exp\left(\tfrac{q(V+IR_s)}{n_1 kT}\right) - 1\right] \\ -I_{sd2}\left[\exp\left(\tfrac{q(V+IR_s)}{n_2 kT}\right) - 1\right] - \tfrac{V+IR_s}{R_{sh}} \end{aligned} \tag{2}$$

where: I_{sd1} and I_{sd2} denote the reverse saturation currents for the dual diodes; n_1 and n_2 are the ideal factors of two diodes.

For the double diode model, seven parameters must be resolved: I_{ph}, I_{sd1}, I_{sd2}, R_s, R_{sh}, n_1 and n_2.

1.3 Photovoltaic module model

Structurally, a photovoltaic module integrates multiple serially-connected solar cells, with its single and double diode models corresponding to (1) and (2) respectively. It only needs to multiply the ideal factor and series parallel resistance by the number of series N_s respectively, which will not be repeated here.

2 Improved crested porcupine optimization algorithm

2.1 Crested porcupine optimization algorithm

Drawing on the crested porcupine's diverse defensive mechanisms, the algorithm computationally emulates four distinct protection strategies to resolve optimization challenges. The population size updates iteratively, after which a specific defensive strategy is selected through comparative assessment of generated random number values. The time complexity of CPO is similar to most other heuristic algorithms, and details can be found in [29].

2.1.1 Cyclic population reduction strategy

By dynamically regulating crested porcupine agent numbers, the method boosts convergence velocity while safeguarding solution diversity. The corresponding model is:

$$N = N_{\min} + (N_{\max} - N_{\min}) \times \left(1 - \left(\frac{t\% \frac{T_{\max}}{T}}{\frac{T_{\max}}{T}}\right)\right) \tag{3}$$

where: N, $N_{\max}$ and $N_{\min}$ are the current, maximum and minimum number of individuals; t is the current iteration index;% denotes the remainder computation operator; $T_{\max}$ is the maximum iteration count; T is the remaining loop iterations.

2.1.2 Visual defense

Under this strategy, the crested porcupine will raise its tail to increase visual volume. When predators approach the porcupine, diminished proximity between them triggers intensified mid-region exploration to accelerate convergence; conversely, predator retreat increases separation, promoting distant area exploration to augment global search efficacy. This behavior is formalized as:

$$\overrightarrow{x_i^{t+1}} = \overrightarrow{x_i^t} + \tau_1 \times \left| 2 \times \tau_2 \times \overrightarrow{x_{\mathrm{CP}}^t} - \frac{\overrightarrow{x_i^t} + \overrightarrow{x_r^t}}{2} \right| \tag{4}$$

where: $\overrightarrow{x_i^t}$ denotes the location of the i-th agent at iteration t; τ_1 represents a Gaussian-distributed random variable; τ_2 signifies a uniformly distributed random number within [0,1]; $\overrightarrow{x_{\mathrm{CP}}^t}$ corresponds to the incumbent optimal solution; r is an integer-valued random number on the interval [1, N].

2.1.3 Sound defense

Under this strategy, the crested porcupine will roar to make noise. As the predator approaches, the sound will become louder, and the predator will choose to approach, stay still or leave according to the size of the noise. This behavior is formalized as:

$$\begin{aligned}\overrightarrow{x_i^{t+1}} = \overrightarrow{U_1} \odot \left(\frac{\overrightarrow{x_i^t} + \overrightarrow{x_r^t}}{2} + \tau_3 \times \left(\overrightarrow{x_{r_1}^t} - \overrightarrow{x_{r_2}^t}\right)\right) \\ + \left(1 - \overrightarrow{U_1}\right) \odot \overrightarrow{x_i^t}\end{aligned} \tag{5}$$

where: $\odot$ is the elements corresponding to the vector are multiplied; r_1 and r_2 are integer-valued random numbers on the interval [1, N]; τ_3 is a random number on the interval [0,1]; $\overrightarrow{U_1}$ is a vector composed of 0 and 1, which is the same as the $\overrightarrow{x_i^t}$ −dimension, used to simulate different situations of the influence of defense strategies on the distance between the catcher and the crested porcupine.

2.1.4 Odor defense

Under this strategy, the crested porcupine secretes a foul-smelling odor that spreads in the surrounding area to deter predators from approaching, with an intensity similar to the predator response and sound defense strategy. This behavior is formalized as:

$$\begin{aligned}\overrightarrow{x_i^{t+1}} = \left[\overrightarrow{x_{r_1}^t} + S_i^t \times \left(\overrightarrow{x_{r_2}^t} - \overrightarrow{x_{r_3}^t}\right) - \tau_3 \times \overrightarrow{U_2} \times \gamma_t \times S_i^t\right] \\ \odot \overrightarrow{U_1} + \left(1 - \overrightarrow{U_1}\right) \odot \overrightarrow{x_i^t}\end{aligned} \tag{6}$$

where: r_3 is a random integer between 1 and N inclusive; $\overrightarrow{U_2}$ is a vector composed of −1 and 1, which is the same as the $\overrightarrow{x_i^t}$ −dimension, used to control the search direction; γ_t is the defense coefficient; S_t^i represents the odor propagation parameter, and their expressions are:

$$\gamma_t = 2 \times \mathrm{rand} \times \left(1 - \frac{t}{T_{\max}}\right)^{\frac{t}{T_{\max}}} \tag{7}$$

$$S_i^t = \exp\left(\frac{f\left(x_i^t\right)}{\sum_{k=1}^{N} f\left(x_k^t\right)}\right) \tag{8}$$

where: $f(x_i^t)$ denotes the individual fitness value corresponding to the i-th member within the t-th evolutionary iteration; rand represents a stochastic value sampled from the range [0,1].

2.1.5 Physical attacks

Under this strategy, the crested porcupine will use burr to attack predators, which is characterized by one-dimensional non-elastic collision. This behavior is formalized as:

$$\begin{aligned}\overrightarrow{x_i^{t+1}} = \overrightarrow{x_{\mathrm{CP}}^t} + [\alpha(1-\tau_4) + \tau_4] \times \left(\overrightarrow{U_1} \odot \overrightarrow{x_{\mathrm{CP}}^t} - \overrightarrow{x_i^t}\right) \\ - \tau_5 \times \overrightarrow{U_1} \times \gamma_t \odot \overrightarrow{\tau_6} \times \frac{S_i^t \times \left(\overrightarrow{x_r^t} - \overrightarrow{x_i^t}\right)}{\Delta t}\end{aligned} \tag{9}$$

where: α is the parameter convergence rate factor; τ_4, τ_5 represents stochastic values sampled from the range [0,1].

$\overrightarrow{\tau_6}$ is a vector including random values generated between 0 and 1.

2.2 Improve the optimization algorithm of crested porcupine

Given the functionally implicit and strongly nonlinear nature of photovoltaic systems, their parameter identification constitutes a multimodal optimization challenge prone to premature convergence at local optima. Therefore, the following two improvement measures are introduced to further enhance the global optimization ability.

2.2.1 Population initialization via chaotic mapping

Chaotic mapping is leveraged to produce chaotic sequences, which exhibit favorable characteristics including nonlinearity, ergodicity, and randomness. Random population initialization often leads to uneven distribution of initial candidate solutions, impeding the algorithm's exploration of global optima. Thus, we use chaos mapping instead of random initialization to improve initial solution quality. Compared with the widely applied Logistic mapping, the Tent mapping has better uniformity but suffers from issues like insufficient uncertain periodic points. Thus, this paper adopts an improved Tent chaos mapping:

$$z_{k+1} = \begin{cases} 2(z_k + 0.1r) & z_k < 0.5 \\ 2 - 2(z_k + 0.1r) & z_k \geqslant 0.5 \end{cases} \tag{10}$$

where: r represents a stochastic value sampled from the range [0,1].

To demonstrate the advantages of the improved Tent chaotic mapping over traditional random initialization, we designed an experiment using two common low-dimensional test functions (Sphere and Rastrigin) for easy visualization and calculation. Generate 50 initial individuals through initialization using the proposed improved Tent chaotic mapping method and traditional random method. The most intuitive "grid coverage method" was used to calculate uniformity: The 2D search space was divided into a 10 × 10 uniform grid (100 grids in total); The number of grids containing initial individuals (denoted as C) was counted for both initialization methods; Uniformity was defined as Uniformity = $C/100$. A value closer to 0.5 indicates a more uniform population distribution. For each test function, each initialization method was run independently 30 times. The average value and standard deviation of uniformity from 30 runs were computed for comparison.

The experimental results are shown in Figs. 2 and 3. It can be seen that the proposed method has significant advantages compared to the random initialization method. The average uniformity of the improved Tent initialization (about 0.42) is significantly higher than that of the random initialization (about 0.37). These results directly demonstrate that the improved Tent chaotic initialization can generate a more uniform initial population, providing more comprehensive spatial coverage for the subsequent search of the ICPO algorithm and avoiding the local aggregation problem of traditional random initialization

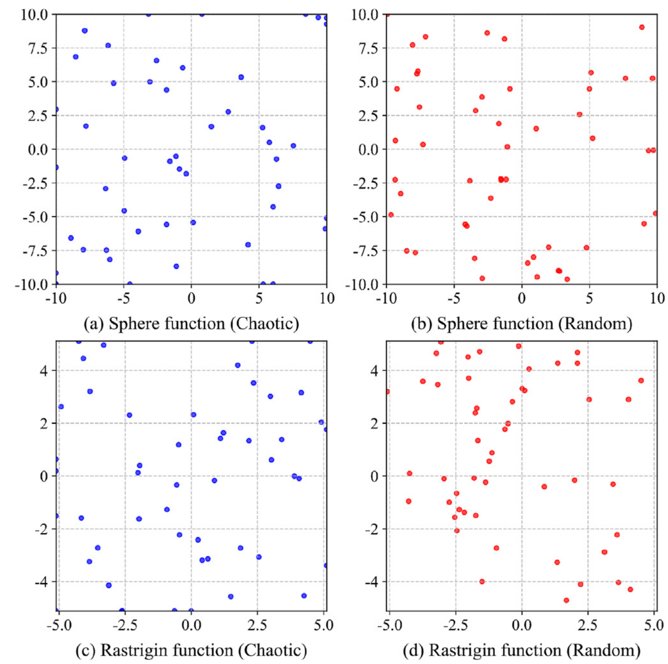

Fig. 2. Comparison of population distribution.

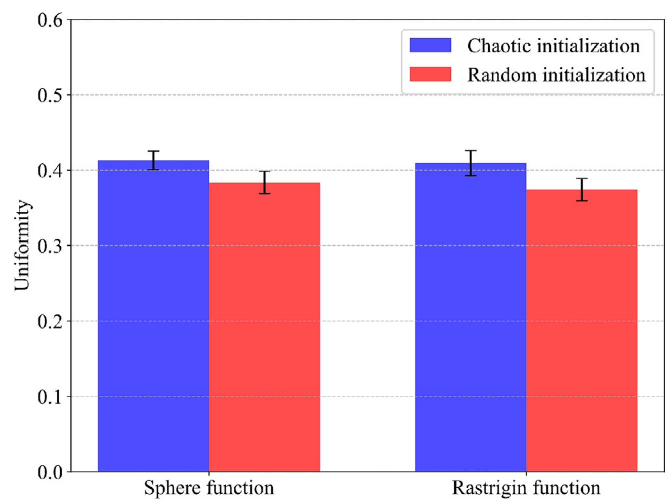

Fig. 3. Comparison of average distribution uniformity.

2.2.2 Levy flight disturbance

Levy flight is a Markov process, a stochastic walking strategy based on the Levy distribution. Its core idea is to simulate the random movement behavior of organisms when searching for food. Unlike ordinary random walks, the step length distribution of Levy flight follows a power-law distribution, enabling long-distance movements. Adding Levy flight perturbations to underperforming individuals helps them escape local optima and enhances the algorithm's global optimization capability. The specific perturbation method is:

$$\begin{cases} x_i' = x_i + \alpha \oplus Levy(\beta) \\ \alpha = \alpha_0(x_i - x_{best}) \\ Levy(\beta) = u/|v|^{1/\beta} \end{cases} \tag{11}$$

where: $\alpha$is the step length control factor; $\oplus$ is the point multiplication symbol; $Levy(\beta)$ denotes the stochastic search trajectory conforming to Levy distribution, where

$$\begin{cases} u \sim N(0, \sigma_u^2), v \sim N(0, \sigma_v^2) \\ \sigma_u = \left[\frac{\Gamma(1+\beta)\times\sin(\pi\beta/2)}{\Gamma((1+\beta)/2)\times 2^{\left(\frac{\beta-1}{2}\right)}\times\beta}\right]^{\frac{1}{\beta}}, \sigma_v = 1 \end{cases} \tag{12}$$

In this paper, α_0 is set to 0.01, and β is set to 1.5. In addition, in order to effectively add disturbance, the inferior crested porcupine with a lower evolutionary degree than the average evolutionary degree of the population is selected for disturbance in the iteration, and its determination formula is:

$$f(x_i^{t+1}) - f(x_i^t) < \frac{1}{N}\sum_{x_i \in N}(f(x_i^{t+1}) - f(x_i^t)) \tag{13}$$

Record the disadvantage of each individual in the iteration, and add the Levy flight disturbance to the crested porcupines that have been disadvantaged for k consecutive generations. In this article, k is taken as 3.

To directly verify the statistical effects of Levy flight disturbances, we conducted a control experiment using standard multimodal test functions (Rastrigin and Griebank) to compare the escape probabilities of pure CPO and ICPO. The experimental design aims to isolate the influence of Levy flight (all other parameters remain consistent) and quantify the differences through statistical indicators. To avoid the randomness of initialization, all experiments were repeated 30 times and the average value was calculated. To statistically compare escape ability, three metrics are defined:

Trapping Probability: The frequency at which individuals are deemed trapped in local optima, defined as the ratio of total trapping events to the maximum possible trapping events. A trap is identified when an individual's fitness change over 10 consecutive generations is less than 0.1 and its fitness remains far from the theoretical optimum (0.001).

Escape Probability: The proportion of trapped individuals that successfully escape local optima, calculated as the ratio of escape events to total trapping events. An escape is confirmed when the fitness reduction after trapping exceeds 0.1.

Mean Escape Generations: The average number of generations required to escape a local optimum, computed as the mean difference between the generation when escape is confirmed and the generation when trapping is detected.

The experimental results are shown in Fig. 4, where all indicators are the average values of 30 repeated runs. It can be seen that the ICPO combined with Levy flight disturbance is significantly enhanced compared to standard CPO:

Reduced trapping probability: Levy flight's random long jumps help individuals avoid stagnation, lowering the likelihood of being trapped in local optima. Higher escape probability: The non-Gaussian step sizes of Levy flight enable more effective breaks from local optima once trapped. Fewer escape generations: The aggressive exploration capability of Levy flight accelerates escape, reducing the average generations needed to break free from local optima.

2.3 Improved crested porcupine optimization algorithm procedure

The improved crested porcupine optimization algorithm introduces chaotic mapping and Levy flight disturbance at the population initialization stage and after one iteration to enhance the algorithm's global optimization capability, as shown in Fig. 5. The fitness function is formulated as the root mean square error computed between the output current of the identification model and the sampled data points.

Algorithm 1 (*Pseudo code of ICPO*).

```
Start
    Set parameters N, T_max, α, T_f, T, N_min, α_0, β;
    Initialize solutions' positions using (10);
  While (t < T_max) do
    Evaluate fitness values for initial solutions;
    Determine the best solution so far (x→^t_CP);
    Update γ_t using (7);
    Update population size using (3);
  For i = 1 to N do
    Generate random numbers τ_8, τ_9
    If τ_8 > τ_9 %% Exploration phase
    Generate random numbers τ_6, τ_7
    If τ_6 > τ_7 %% First defense mechanism
    Apply (4)
    Else %% Second defense mechanism
    Apply (5)
    Else %% Exploitation phase
    If τ_10 < T_f: %% Third defense mechanism
    Apply (6)
    Else %% Fourth defense mechanism
    Apply (9)
  End if
  End for
  Identify disadvantaged individuals by (13)
  Add disturbances to the disadvantaged individuals according to (11)
  t = t+1
  End while
  Return x→^t_CP
STOP
```

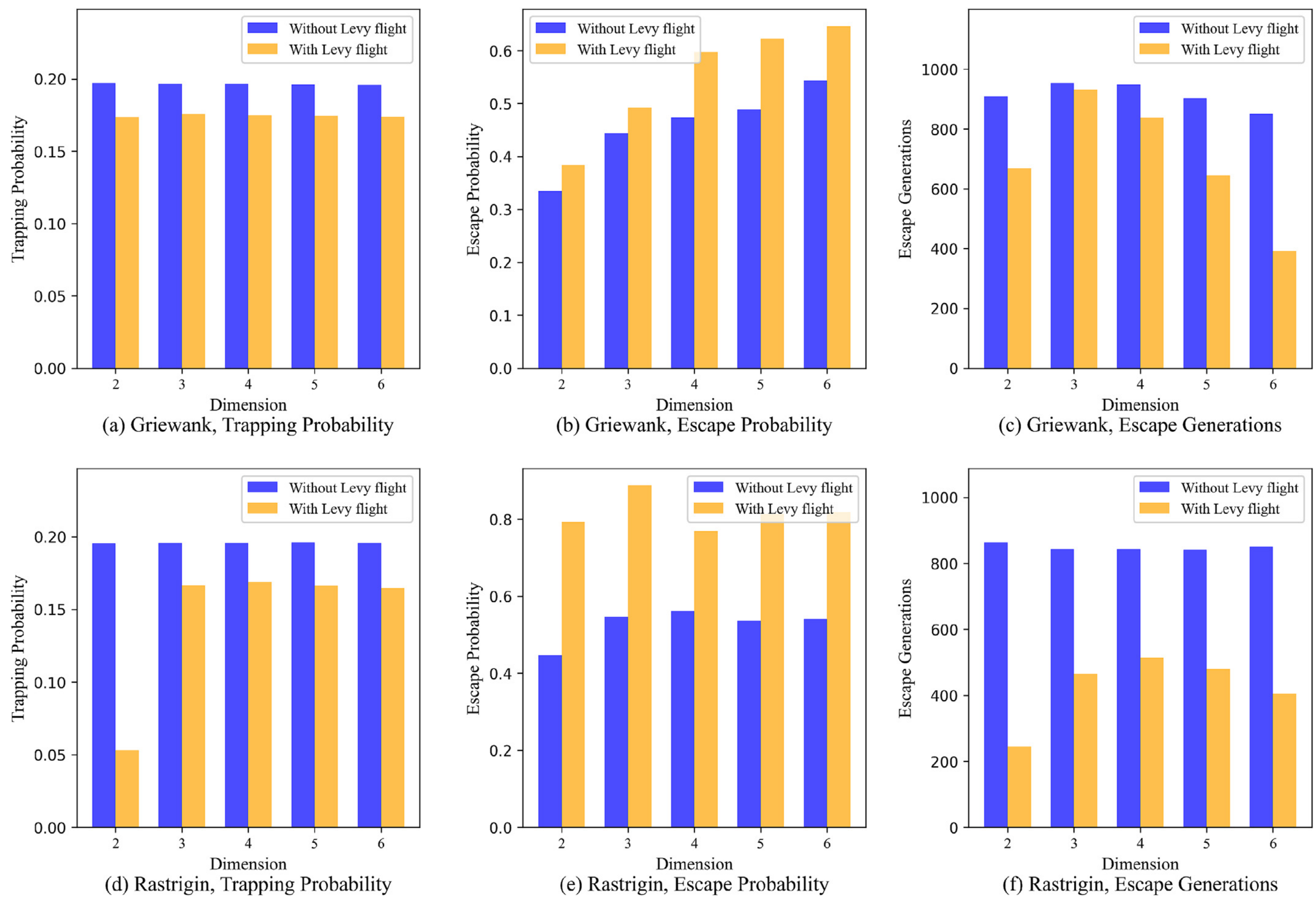

Fig. 4. The comparison results of whether to include levy flight disturbance.

3 Experimental verification and analysis

3.1 Case and algorithm settings

To systematically assess the effectiveness and comparative advantages of the newly developed ICPO algorithm regarding PV parameter identification, we employ four distinct validation scenarios: SDM-RTC, DDM-RTC, SDM-PWP201, and DDM-PWP201, which are referred to as Case 1, 2, 3, and 4, respectively. Here, RTC represents 26 sets of measured data from a market-available silicon photovoltaic cell measuring 57 mm in diameter under 1000 W/m^2 and 33℃ conditions, while PWP201 represents 25 sets of measured data from a Photowatt-PWP201 commercial photovoltaic module composed of 36 multicrystalline silicon cells under 1000 W/m^2 and 45℃ conditions. Both are widely used in relevant research validation processes to facilitate comparison between existing methods and the proposed method. SDM and DDM estimate parameters using single-diode and dual-diode models, respectively, with a key distinction in the quantity of parameters requiring identification: 5 parameters for the former and 7 for the latter, which renders the latter more computationally challenging. The parameter identification ranges for RTC and PWP201 are shown in Table 1. It is important to highlight that this paper incorporates the quantity of series-connected battery cells into the model, thereby ensuring that the parameter range within the photovoltaic module remains relatively stable.

To compare the identification effects of different methods, the algorithms CPO (Crested Porcupine Optimizer), GWO (Grey Wolf Optimization), WOA (Whale Optimization Algorithm), TSO (Tuna Swarm Optimization), and ZOA (Zebra Optimization Algorithm) were used for comparison. The parameter configurations for each algorithm are presented in Table 2, where the ZOA algorithm has no hyperparameters. All algorithms have 30 individuals, 5000 iterations, and are repeated 30 times to avoid random effects.

To comprehensively assess the effectiveness of diverse algorithms, three primary evaluation metrics are utilized, including Root Mean Square Error (RMSE) which enables intuitive comparison of identification outcomes.; Variance, which characterizes algorithm stability; and the iteration count needed for the mean fitness to attain the target fitness level (NFFE), which quantifies the algo-

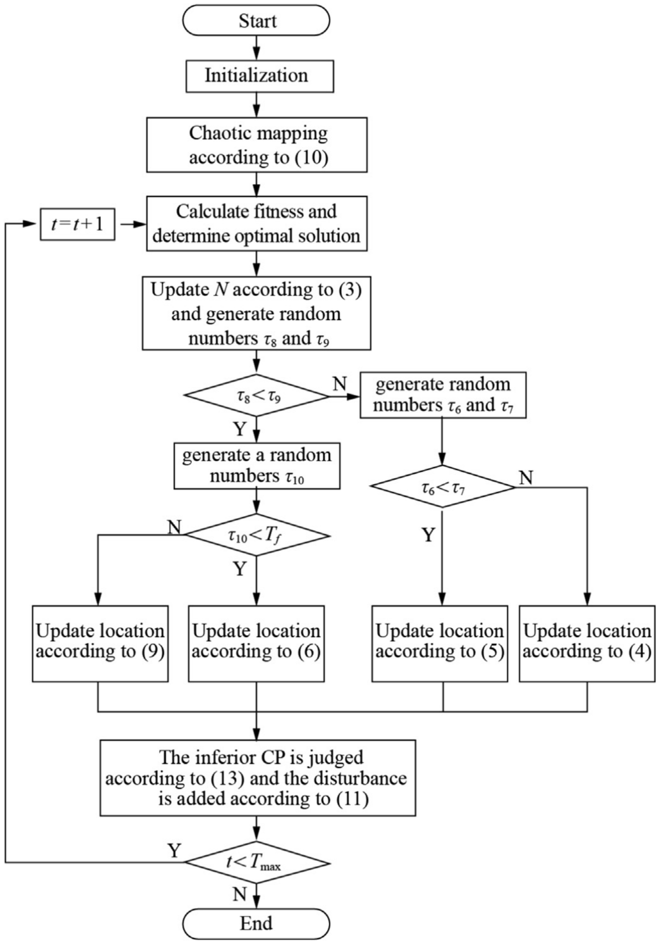

Fig. 5. Flowchart of the Improved Crested Porcupine Optimizer (ICPO) algorithm.

Table 1
Range of parameter identification.

Parameter	RTC	PWP201
I_{ph}/A	0∼1	0∼2
I_{sd} 、I_{sd1} 、I_{sd2}/μA	0.1∼1	0.1∼10
R_s/Ω	0∼0.5	0∼0.75
R_{sh}/ Ω	0∼100	0∼150
n 、n_1 、n_2	1∼2	1∼2

Table 2
Parameter setting for optimization algorithms.

Algorithm	Parameters
ICPO	$T_f = 0.6$, $T = 2$, $\alpha = 0.1$, $N_{min} = 20$, $\alpha_0 = 0.01$, $\beta_0 = 1.5$, $k = 3$
CPO	$T_f = 0.6$, $T = 2$, $\alpha = 0.1$, $N_{min} = 20$
GWO	$a = 2$∼0
WOA	$a = 2$∼0, $b = 1$
TSO	$z = 0.05$, $a = 0.7$

rithm's convergence rate. The Success Rate (SR) is characterized as the likelihood that the final fitness value falls below the predefined target threshold, which reflects the algorithm's dependability. The expected fitness for RTC and PWP201 is set at 0.003 and 0.005, respectively.

In addition, the proposed method was fully verified by comparing the methods in related literatures using the same data set, and the model accuracy was evaluated by RMSE.

3.2 Experimental results and analysis

Average fitness convergence trajectories of diverse optimization algorithms across various scenarios are depicted in Fig. 6. Visual inspection of these plots reveals that the proposed ICPO algorithm demonstrates notable enhancement, consistently outperforming all other curves throughout the entire process with the swiftest convergence velocity and most robust global optimization capability.

The three proposed performance metrics evaluated different optimization algorithms. Table 3 results demonstrate the proposed approach's strengths in global optimization, convergence speed, stability, and reliability. The RMSE of ICPO is 10% to 30% lower than that of CPO in four different scenarios, and over 85% lower than other advanced algorithms. ICPO has an order of magnitude advantage over other algorithms in terms of variance of RMSE. A Wilcoxon signed-rank test with a significance level of 0.05 is used to compare the average results from 30 runs for each algorithm. All check symbols in Table 3 are '+' indicating that there are significant differences in all test instances between ICPO and the comparison algorithms. Notably, the ZOA algorithm performed the worst in all cases, indicating that while novel high-performance algorithms excel in some test functions, they may not perform

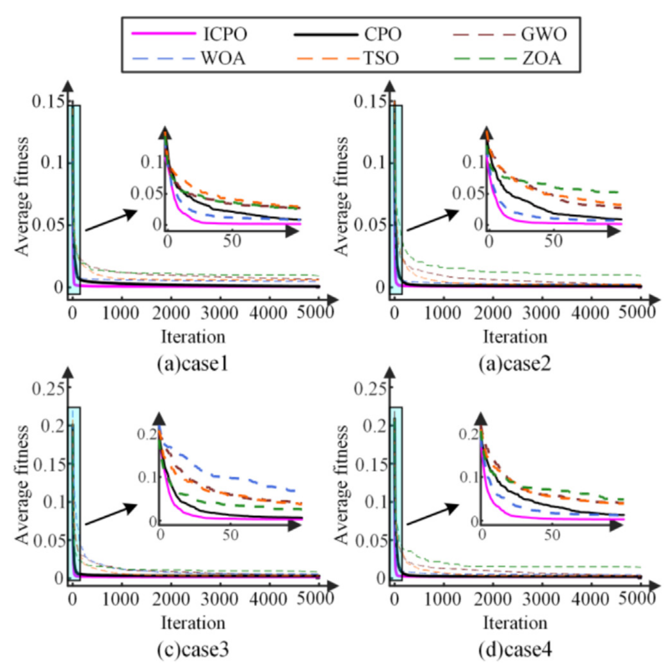

Fig. 6. The average fitness convergence curves.

Table 3
Evaluation results of different algorithms.

Case	Algorithm	RMSE			NFFE	SR	Time/s
		Mean	Variance	Sig.			
1	ICPO	7.7307×10^{-4}	1.1086×10^{-13}	+	33	30/30	505.32
	CPO	8.5164×10^{-4}	6.6938×10^{-9}	+	1070	30/30	467.67
	GWO	6.6409×10^{-3}	2.1558×10^{-5}	+	>5000	5/30	446.53
	WOA	4.7679×10^{-3}	5.0966×10^{-7}	+	>5000	1/30	470.40
	TSO	6.0251×10^{-3}	2.8296×10^{-6}	+	>5000	2/30	466.36
	ZOA	9.1457×10^{-3}	1.6252×10^{-5}	+	>5000	0/30	886.40
2	ICPO	7.8716×10^{-4}	1.7582×10^{-8}	+	47	30/30	762.17
	CPO	9.7661×10^{-4}	3.8702×10^{-8}	+	234	30/30	704.89
	GWO	1.8460×10^{-3}	3.3208×10^{-7}	+	4128	30/30	587.64
	WOA	2.4982×10^{-3}	3.2674×10^{-7}	+	1877	23/30	631.09
	TSO	2.3888×10^{-3}	4.7493×10^{-7}	+	1541	25/30	626.05
	ZOA	9.3379×10^{-3}	4.0768×10^{-5}	+	>5000	5/30	1149.05
3	ICPO	2.0546×10^{-3}	7.0902×10^{-11}	+	38	30/30	588.71
	CPO	3.1165×10^{-3}	6.5239×10^{-8}	+	209	30/30	560.28
	GWO	3.6761×10^{-3}	1.4378×10^{-6}	+	3955	25/30	476.01
	WOA	5.5888×10^{-3}	6.4712×10^{-6}	+	>5000	17/30	543.55
	TSO	3.3307×10^{-3}	2.2635×10^{-6}	+	1253	27/30	490.26
	ZOA	8.3773×10^{-3}	5.3240×10^{-5}	+	>5000	13/30	915.52
4	ICPO	2.1453×10^{-3}	2.0041×10^{-8}	+	43	30/30	921.45
	CPO	2.2297×10^{-3}	3.1544×10^{-8}	+	222	30/30	814.80
	GWO	3.5251×10^{-3}	2.3556×10^{-6}	+	3972	25/30	610.90
	WOA	4.5066×10^{-3}	5.7119×10^{-7}	+	2498	22/30	792.30
	TSO	3.4041×10^{-3}	1.5600×10^{-6}	+	1360	28/30	651.46
	ZOA	1.4421×10^{-2}	8.5112×10^{-5}	+	>5000	8/30	1277.33

well in real-world engineering problems. Further exploration is needed to find the most suitable optimization algorithm for specific problems.

Table 4 lists the parameters estimated by the proposed method and the relevant RMSE values for each scenario. The results indicate that the ICPO algorithm has significant advantages over existing methods and can achieve higher precision parameter estimation results in all cases. Compared with existing methods, the error is significantly reduced by about 20%.

The I-V curves of each case model identified by the proposed ICPO algorithm are shown in Fig. 7. Visual inspection of the results indicates that all four cases exhibit close alignment with the experimental data points, thereby substantiating the efficacy of the proposed method.

Notably, case analysis shows that while the double diode model more precisely captures the inherent physical properties of photovoltaic systems relative to the single diode configuration, its practical simulation accuracy demonstrates no significant improvement, and identification stability declines. Root cause stems from the double diode configuration's greater complexity and requirement for identifying a larger number of parameters, which results in reduced precision in parameter estimation. Clearly, the single-diode model proves more appropriate for the practical photovoltaic cells and modules examined in this study.

3.3 Analysis of parameter uncertainty and global convergence

To further validate the robustness of ICPO and quantify the uncertainty of identified parameters, we conducted a bootstrap-based uncertainty analysis. For each case, 30 independent runs of ICPO were performed to generate a sample set of parameter estimates. Calculate the average value and standard deviation (SD) of the parameters obtained from 30 parameter identifications. For each parameter, 1000 bootstrap samples were resampled with replacement from the 30 estimates, and 95% confidence intervals (CIs) were derived from the 2.5th and 97.5th percentiles of the bootstrap distribution. The uncertainty analysis results are summarized in Table 5 and confirm that ICPO provides stable parameter estimates with tight confidence intervals, supporting its reliability in practical applications.

To investigate whether the proposed ICPO algorithm converges to the global optimum or approaches the global optimum region, a supplementary brute force search experiment was designed to verify the closeness between the ICPO solution and the theoretical global optimum solution.

Brute-force search is an exhaustive optimization method that explores all possible parameter combinations within a predefined search space, making it a reliable benchmark for validating global optimality—provided

Table 4
Results of parameter identification using different methods.

Case	Algorithm	Parameter							RMSE
		I_{ph}/A	I_{sd}、I_{sd1}/μA	I_{sd2}/μA	R_s/ Ω	R_{sh}/ Ω	n、n_1	n_2	
1	ICPO	0.7608	0.3107		0.0365	52.8909	1.4773		7.7730×10^{-4}
	RLGSK [19]	0.7608	0.3230		0.0364	53.7185	1.4812		9.8603×10^{-4}
	DE3P [20]	0.7607	0.3191		0.0363	54.1924	1.4798		8.1291×10^{-4}
	TLABC [21]	0.7608	0.3230		0.0364	53.7164	1.4811		9.8602×10^{-4}
	GOTLBO [22]	0.7608	0.3316		0.0363	54.1154	1.4838		9.8744×10^{-4}
	NM-MPSO [23]	0.7608	0.3231		0.0364	53.7222	1.4812		9.8602×10^{-4}
	DPDE [24]	0.7607	0.3230		0.0363	53.7185	1.4811		8.8602×10^{-4}
	WHHO [25]	0.7608	0.3230		0.0364	53.7187	1.4811		9.8602×10^{-4}
2	ICPO	0.7608	0.1762	0.9748	0.0372	55.0322	1.4299	1.9729	7.4740×10^{-4}
	RLGSK [19]	0.7608	0.2259	0.7499	0.0367	55.4823	1.4510	2	9.8252×10^{-4}
	TLABC [21]	0.7608	0.2401	0.4239	0.0367	54.6680	1.4567	1.9075	9.8415×10^{-4}
	GOTLBO [22]	0.7608	0.2205	0.8002	0.0368	56.0753	1.4490	2	9.8318×10^{-4}
	NM-MPSO [23]	0.7608	0.2248	0.7552	0.0368	55.5296	1.4505	2	9.8250×10^{-4}
	DPDE [24]	0.7608	0.2260	0.7495	0.0367	55.4870	1.4510	2	9.8248×10^{-4}
	WHHO [25]	0.7608	0.2286	0.7272	0.0367	55.4264	1.4519	2	9.8249×10^{-4}
3	ICPO	1.0314	2.6391		0.0343	22.8291	1.3222		2.0530×10^{-3}
	RLGSK [19]	1.0305	3.4823		0.0334	27.2773	1.3512		2.4251×10^{-3}
	DE3P [20]	1.0335	2.1248		0.0347	19.3720	1.3002		2.4227×10^{-3}
	TLABC [21]	1.0306	3.4715		0.0334	27.0260	1.3509		2.4251×10^{-3}
	NM-MPSO [23]	1.0305	3.6817		0.0332	27.3333	1.3572		2.3564×10^{-3}
	WHHO [25]	1.0305	3.4821		0.0334	27.2751	1.3500		2.4251×10^{-3}
	CIJAYA [26]	1.0305	3.4823		0.0334	27.2773	1.3519		2.4251×10^{-3}
4	ICPO	1.0314	0.1004	2.6282	0.0343	22.8421	1.3218	1.9999	2.0540×10^{-3}
	TLABC [21]	1.0331	1.5280	2.6762	0.0343	19.8736	1.2832	1.5499	2.2138×10^{-3}
	WHHO [25]	1.0324	1×10^{-6}	2.5129	0.0344	20.6865	1.3169	1.3173	2.0663×10^{-3}
	STLBO [27]	1.0328	1.6899	2.5708	0.0337	19.7860	1.3218	1.7314	2.2785×10^{-3}

computational feasibility is ensured. However, PV model parameter identification faces the curse of dimensionality: for a 5-parameter single-diode model (SDM), a brute-force search with a precision of 10^{-3} for each parameter would require over 10^{15} parameter combinations. For higher dimensional models and higher search accuracy, this number will grow exponentially, exceeding actual time and memory limitations.

To mitigate this, the experiment focused on Case 1 and Case 3. Specifically, three parameters (I_{ph}, R_s, n) were fixed at the values identified by ICPO (retained to four significant figures), while the remaining two parameters I_{sd} and R_{sh}—were subjected to brute force search with accuracies of 10^{-4} and 10^{-3}. This design balances computational feasibility and the ability to validate convergence toward the global optimum. The brute-force search results for Cases 1 and 3 are presented in the Fig. 8.

It is not difficult to see from Fig. 7 that the optimal parameter pairs identified through brute force search are located near the corresponding parameters obtained by ICPO. This directly confirms that the solution of ICPO is located within the global optimal region, as exhaustive search did not find a better parameter subspace within the range recognized by ICPO. In summary, despite the computational limitations of brute-force search (restricted to 2-dimensional subspace), its results explicitly demonstrate that ICPO converges to a solution close to the global optimum.

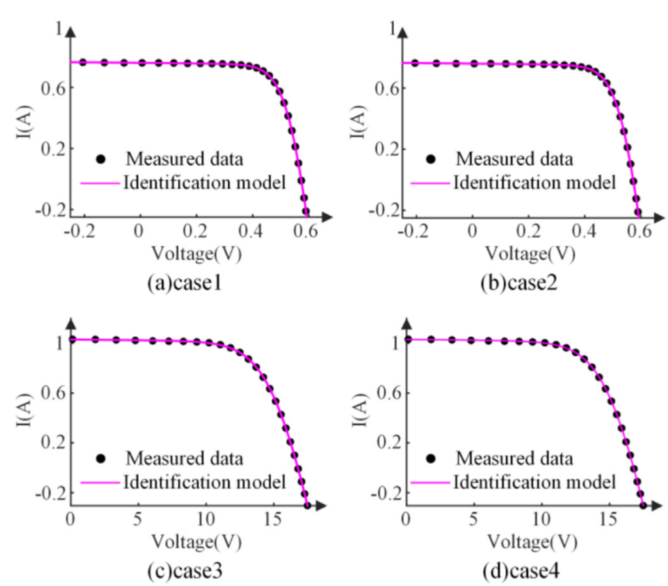

Fig. 7. I-V curves for each case.

Table 5
Parameter uncertainty results via bootstrap method.

Case	Parameter	Mean	SD	95% CI	Case	Parameter	Mean	SD	95% CI
1	I_{ph}/A	0.76080	7.48×10^{-5}	(0.76078, 0.76083)	3	I_{ph}/A	1.03146	1.62×10^{-4}	(1.03142, 1.03152)
	I_{sd}/μA	0.30362	0.0378	(0.29010, 0.31714)		I_{sd}/μA	2.63659	0.0121	(2.63163, 2.63988)
	R_s/ Ω	0.03670	8.31×10^{-4}	(0.03655, 0.03716)		R_s/ Ω	0.03432	5.73×10^{-6}	(0.03432, 0.03433)
	R_{sh}/ Ω	52.3545	2.8534	(51.2892, 52.8898)		R_{sh}/ Ω	22.7785	0.3489	(22.6423, 22.8626)
	n	1.47374	0.0189	(1.46671, 1.47727)		n	1.32212	4.60×10^{-4}	(1.32194, 1.32225)
2	I_{ph}/A	0.76075	1.43×10^{-4}	(0.76070, 0.76079)	4	I_{ph}/A	1.03135	4.97×10^{-4}	(1.03114, 1.03151)
	I_{sd1}/μA	0.16719	0.0524	(0.14957, 0.18619)		I_{sd1}/μA	0.38933	0.4030	(0.24837, 0.53690)
	I_{sd2}/μA	0.54138	0.2949	(0.44274, 0.65362)		I_{sd2}/μA	2.35350	0.4786	(2.17604, 2.52116)
	R_s/ Ω	0.03693	5.16×10^{-4}	(0.03675, 0.03712)		R_s/ Ω	0.03431	1.52×10^{-4}	(0.03426, 0.03437)
	R_{sh}/ Ω	54.2986	2.0235	(53.6080, 55.0201)		R_{sh}/Ω	23.2209	1.9900	(22.6314, 24.0775)
	n_1	1.44076	0.0236	(1.43235, 1.44905)		n_1	1.30448	0.0322	(1.29160, 1.31438)
	n_2	1.85083	0.1640	(1.78779, 1.90111)		n_2	1.49344	0.2462	(1.41128, 1.58575)

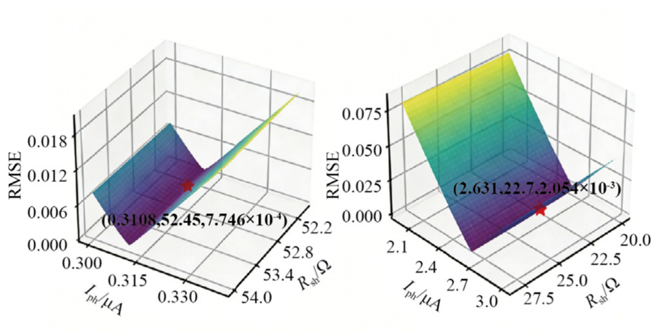

Fig. 8. Brute force search results.

4 Conclusion

To address PV equivalent circuit model parameter estimation, this study proposes the ICPO algorithm for photovoltaic model parameter identification. Applying it to four cases with two models and two datasets, and comparing it with other algorithms and existing research, validates its efficacy and superior performance. Based on the analysis, the key conclusions can be summarized as follows:

1) In the four cases, the model parameters identified by ICPO algorithm can fit the measured data well, so it is effective to use ICPO algorithm for photovoltaic model parameters.
2) In contrast to alternative optimization algorithms, the proposed ICPO algorithm demonstrates remarkable strengths in global optimization capability, convergence rate, and operational stability, while manifesting pronounced benefits in photovoltaic model parameter estimation.
3) Compared with the existing research results, the proposed ICPO algorithm can achieve higher model accuracy in four cases, and make significant progress in the identification accuracy of photovoltaic model parameters.

CRediT authorship contribution statement

Hao Guo: Writing – review & editing, Writing – original draft. **Chongru Liu:** Supervision, Project administration, Conceptualization.

Declaration of competing interest

The authors declare that they have no known competing financial interests or personal relationships that could have appeared to influence the work reported in this paper.

Acknowledgments

This work was supported by the National Natural Science Foundation of China under Grant U23B6008

References

[1] G.P. Chen, Y. Dong, Z.F. Liang, Analysis and reflection on high-quality development of new energy with Chinese characteristics in energy transition, Proc. CSEE 40 (17) (2020) 5493–5506.
[2] R.X. Fan, G.M. Yin, J.R. Miao, et al., A quick mppt method of pv panel based on parameter identification, Acta Energiae Solaris Sinica 41 (2) (2020) 296–302.
[3] Y.J. Wu, Z.C. Liu, Y.L. Wang, Parameter identification of solar cell model based on ipoa, Acta Energiae Solaris Sinica 45 (1) (2024) 1–10.
[4] A.A. Cárdenas, M. Carrasco, F. Mancilla-David, et al., Experimental parameter extraction in the single-diode photovoltaic model *via* a reduced-space search, IEEE Trans. Ind. Electron. 64 (2) (2017) 1468–1476.
[5] L.E. Peñaranda Chenche, O.S. Hernandez Mendoza, E.P. Bandarra Filho, Comparison of four methods for parameter estimation of mono- and multi-junction photovoltaic devices using experimental data, Renew. Sustain. Energy Rev. 81 (2018) 2823–2838.
[6] N.T. Tong, W. Pora, A parameter extraction technique exploiting intrinsic properties of solar cells, Appl. Energy 176 (2016) 104–115.

[7] A. Ayang, R. Wamkeue, M. Ouhrouche, et al., Maximum likelihood parameters estimation of single-diode model of photovoltaic generator, Renew. Energy 130 (2019) 111–121.
[8] A. Chatterjee, A. Keyhani, D. Kapoor, Identification of photovoltaic source models, IEEE Trans. Energy Convers. 26 (3) (2011) 883–889.
[9] F.J. Toledo, J.M. Blanes, V. Galiano, Two-step linear least-squares method for photovoltaic single-diode model parameters extraction, IEEE Trans. Ind. Electron. 65 (8) (2018) 6301–6308.
[10] C. Zhu, C.X. Zhou, J.Z. Li, et al., Parameter identification of photovoltaic modules based on linear optimization algorithm, Acta Energiae Solaris Sinica 45 (8) (2024) 391–397.
[11] M. Eslami, B. Babaei, H. Shareef, et al., Optimum design of damping controllers using modified sperm swarm optimization, IEEE Access 9 (2021) 145592–145604.
[12] A. Toolabi Moghadam, M. Aghahadi, M. Eslami, et al., Adaptive rat swarm optimization for optimum tuning of SVC and PSS in a power system, Int. Trans. Electr. Energy Syst. 2022 (2022) 4798029.
[13] A. Samadi-Koucheksaraee, X.F. Chu, Development of a novel modeling framework based on weighted kernel extreme learning machine and ridge regression for streamflow forecasting, Sci. Rep. 14 (2024) 30910.
[14] S. Shirvani-Hosseini, A. Samadi-Koucheksaraee, I. Ahmadianfar, et al., Data mining methods for modeling in water science, in: Computational Intelligence for Water and Environmental Sciences, Springer Nature, Singapore, 2022, pp. 157–178.
[15] A. Samadi-Koucheksaraee, S. Shirvani-Hosseini, I. Ahmadianfar, et al., Optimization algorithms surpassing metaphor, in: Computational Intelligence for Water and Environmental Sciences, Springer Nature, Singapore, 2022, pp. 3–33.
[16] Y. Fang, I. Ahmadianfar, A. Samadi-Koucheksaraee, et al., An accelerated gradient-based optimization development for multi-reservoir hydropower systems optimization, Energy Rep. 7 (2021) 7854–7877.
[17] I. Ahmadianfar, W.Y. Gong, A.A. Heidari, et al., Gradient-based optimization with ranking mechanisms for parameter identification of photovoltaic systems, Energy Rep. 7 (2021) 3979–3997.
[18] A. Samadi-koucheksaraee, I. Ahmadianfar, O. Bozorg-Haddad, et al., Gradient evolution optimization algorithm to optimize reservoir operation systems, Water Resour. Manag. 33 (2) (2019) 603–625.
[19] G.J. Xiong, Z.Y. Gu, Reinforcement learning-based Gaining-sharing knowledge algorithm for parameter identification of solar cell models, Acta Energiae Solaris Sinica 45 (9) (2024) 334–434.
[20] V.J. Chin, Z. Salam, A new three-point-based approach for the parameter extraction of photovoltaic cells, Appl. Energy 237 (2019) 519–553.
[21] X. Chen, B. Xu, C.L. Mei, et al., Teaching–learning–based artificial bee colony for solar photovoltaic parameter estimation, Appl. Energy 212 (2018) 1578–1588.
[22] X. Chen, K.J. Yu, W.L. Du, et al., Parameters identification of solar cell models using generalized oppositional teaching learning based optimization, Energy 99 (2016) 170–180.
[23] N.F.A. Hamid, N.A. Rahim, J. Selvaraj, Solar cell parameters identification using hybrid Nelder-Mead and modified particle swarm optimization, J. Renew. Sustain. Energy 8 (2016) 015502.
[24] S.C. Gao, K.Y. Wang, S.C. Tao, et al., A state-of-the-art differential evolution algorithm for parameter estimation of solar photovoltaic models, Energ. Conver. Manage. 230 (2021) 11378.
[25] M. Naeijian, A. Rahimnejad, S.M. Ebrahimi, et al., Parameter estimation of PV solar cells and modules using Whippy Harris Hawks Optimization Algorithm, Energy Rep. 7 (2021) 4047–4406.
[26] X.Z. Jian, Z.Y. Weng, R.Z. Wang, Cijaya algorithm for parameters identification of photovoltaic module model, Acta Energiae Solaris Sinica 42 (11) (2021) 19–112.
[27] Q. Niu, H.Y. Zhang, K. Li, An improved TLBO with elite strategy for parameters identification of PEM fuel cell and solar cell models, Int. J. Hydrogen Energy 39 (8) (2014) 3837–3854.
[28] B. Arandian, M. Eslami, S.A. Khalid, et al., An effective optimization algorithm for parameters identification of photovoltaic models, IEEE Access 10 (2022) 34069–34084.
[29] M. Abdel-Basset, R. Mohamed, M. Abouhawwash, Crested porcupine optimizer: a new nature-inspired metaheuristic, Knowl.-Based Syst. 284 (2024) 111257.

Hao Guo received B.S. degree at North China Electric Power University in Beijing, China, in 2019. He is working towards master's degree at North China Electric Power University in Beijing, China. His research interests include equivalent modeling of new energy power plants.